Size-dependent Effects on the Vibration Behavior of a Timoshenko Microbeam subjected to Pre-stress Loading based on DQM

M. Mohammadimehr*, H. Mohammadi Hooyeh, H. Afshari, M.R. Salarkia

Department of Solid Mechanics, Faculty of Mechanical Engineering, University of Kashan, Kashan, Iran

ABSTRACT

In this paper, size-dependent effects on the vibration behavior of Timoshenko microbeams under pre-stress loading embedded in an elastic foundation, using modified strain gradient theory (MSGT) and surface stress effects, were studied. To consider the surface stress effects, the Gurtin–Murdoch continuum mechanical approach was employed. Using Hamilton's principle, the governing equations of motion and boundary conditions were obtained and solved numerically using the differential quadrature method (DQM). The effects of pre-stress loading, surface residual stress, surface mass density, Young's modulus applied to the surface layer, three material length scale parameters, and the elastic foundation coefficients were investigated. For higher aspect ratios, this study found that the effect of the pre-stress loading was negligible for higher modes. Considering size-dependent effects led to increase the stiffness of the matrix and enhance the dimensionless natural frequencies of the Timoshenko microbeam. The MSGT results were higher than those found using other theories. In addition, this research discovered that there were negligible surface stress effects with each of the three material length scale parameters.

1. Introduction

Nano technology is one of the most powerful technologies that can produce many materials and devices across a range of applications, such as electronics, biomaterials, medicine, and energy production [1-3]. Vibration analysis of composite beams has been a research topic in many engineering fields because vibration plays an important role in the design of turbine blades, helicopter blades, propeller blades, drill bits, and fluted cutters. In practice, these structures are typically modeled as either Euler or Timoshenko beams. The design of micro- and nano-electro-mechanical systems (MEMS/NEMS) requires widespread use of micro-rods and microbeams with different complex behaviors. Currently, micro-composite beams are employed in micro-turbo machines, ultrasonic piezoelectric micromotor designs, and medical micro devices.

Recently, many researchers have investigated the mechanical behaviors of micro- and nano-scale materials using beam, plate, and shell theories. Ghorbanpour Arana et al. [4] analyzed the pulsating fluid-induced dynamic instability of double-walled carbon nano-tubes (DWCNTs), based on a sinusoidal strain gradient theory using the differential quadrature method (DQM) and the Bolotin method. Their results depicted that the imposed magnetic field was an effective controlling parameter for dynamic instability of visco-DWCNTs. In another work, Ghorbanpour Arani et al. [5] presented the nonlinear vibration of coupled nano- and microstructures conveying fluid flow based on a Timoshenko beam model under a two-dimensional magnetic field. They expressed that the magnetic field played an important role in the stability of the carbon nano-tubes (CNTs) and controls the stability of the nanosystem.

---

*Corresponding author, Tel: +98-31-55912423, Fax: +98-31-55912424

E-mail address: mmohammadimehr@kashanu.ac.ir

Simsek [6] studied the free vibration analysis of nanobeams with various boundary conditions, based on the nonlocal elasticity theory for large amplitude. In that research, the effect of nonlocal parameters on the nonlinear frequency ratio was examined. Their results showed that the nonlocal effects should be considered in the analysis of the mechanical behavior of nanostructures. Sahmani and Bahrami [7] analyzed the dynamic stability of microbeams subjected to piezoelectric voltage, using the strain gradient theory (SGT). In their results, for a special value of applied piezoelectric voltage, increasing the dimensionless length scale parameter decreased the difference between stability responses predicted by the classical and non-classical beam models. In addition, Mohammadimehr and Golzari [8] investigated the elliptic phenomenon effect of cross-sections on the torsional buckling of a nano-composite beam reinforced by a single-walled carbon nanotube (SWCNT). With an increase in the matrix thickness, the tangential and longitudinal strains of SWCNT decreased, and the opposite effect occurred for the interface stress and the dimensionless stress of the outer surface.

Alternately, Mohammadimehr and Rahmati [9] considered the small-scale effects on electro-thermo-mechanical vibration analysis of a single-walled boron nitride nanorod under electric excitation. They represented that the natural frequency decreased with an increase in the small-scale effects or aspect ratios. On the other hand, the small-scale effects were significant for lower aspect ratios and higher natural frequencies. Atabakhshian et al. [10] employed vibration of a smart coupled electro-thermal nanobeam system with an internal flow, based on nonlocal elasticity theory, while Ansari et al. [11] derived free vibration analysis from the evaluation of single and double-walled carbon nanotubes based on nonlocal elastic shell models. They concluded that the small-scale effects in the non-local model made nanotubes more flexible. Akgoz and Civalek [12] studied higher-order shear deformation in microbeam models, based on the strain gradient elasticity theory. Their results showed that microbeams derived from the non-classical theories, specifically modified strain gradient theory (MSGT), were stiffer than those based on the classical theory (CT).

Asgharifard Sharabiani and Haeri Yazdi [13] illustrated the nonlinear free vibrations for functionally graded (FG) nanobeams, including their surface effects. The results showed that the surface effects at higher volume fraction indices were either less or more dominant, in small and large amplitude ratios, respectively. Ke et al. [14] investigated the nonlinear vibrations of piezoelectric nanobeams based on the nonlocal and the Timoshenko beam theories.

Their results demonstrated that a change in the external electric voltage from a positive value to a negative value led to a decrease in the nonlinear frequency ratio. Ansari et al. [15] analyzed the bending, buckling, and free vibration responses of FG Timoshenko microbeams, and they observed that the critical buckling loads and natural frequencies predicted by the beam models, based on MSGT and CT, provided the maximum and minimum values, respectively. Tounsi et al. [16] illustrated size-dependent bending and vibration analysis of FG microbeams, based on MCST and neutral surface positions. They represented that the inclusion of the couple stress effect makes a microbeam stiffer and decreased the vertical displacement and increased the natural frequency.

Alternately, Nazemnezhad et al. [17] employed an analytical study on the nonlinear free vibration of nanoscale beams incorporating surface density effects. They observed that the effect of the surface density on the variation of the natural frequency of the nanobeam versus the thickness ratio decreases consistently with the increase of the mode number. Nejat Pishkenari et al. [18] examined the surface elasticity and size effects on the vibrational behavior of silicon nanoresonators. They developed a continuum model for nanobeam vibrations that was capable of predicting the results of molecular dynamics (MD) simulations with considerably lower computational effort. Yue et al. [19] proposed a microscale Timoshenko beam model for piezoelectricity using flexoelectricity and surface effects. Their results observed that the change of surface properties not only directly affected the static bending but also significantly changed the natural frequency of the beam. Preethi et al. [20] presented surface and non-local effects of the nonlinear analysis of Timoshenko beams using Eringen's nonlocal theory and the Gurtin-Murdoch approach, where the nonlocal parameters and the positive surface parameters' values decreased the stiffness of the beam and resulted in larger deflections and lower frequencies.

In this research, a Timoshenko microbeam model, based on the modified strain gradient theory (MSGT) and surface stress effects subjected to pre-stress loading, is presented. The MSGT and surface stress effects were considered together in this study because both of them affect the structure at the microscale. Despite the fact that the surface and small scale effects have been investigated individually in some papers, the novelty of this study lies in the evaluation of size-dependent effects, including three material length scale parameters, and the surface residual stress based on strain gradient, and the surface stress elasticity effects on the dimensionless natural frequency of Timoshenko microbeams, subjected to pre-stress loading and considered simulta-

neously at a microscale. Moreover, the size-dependent effects increased the dimensionless natural frequency due to increasing flexural rigidity, which then enhanced the stability of the microstructures. The governing equations of motion were obtained using Hamilton's principle and energy method. The equations were solved using the differential quadrature method (DQM).

2. The Governing Equations of Timoshenko microbeams

A schematic view of a straight Timoshenko microbeam model based on surface layers, an elastic medium, and pre-stress load is shown in Figure 1. The displacement fields for this model can be stated as [21]

$$u(x,z,t) = u_0(x,t) - z\psi_0(x,t) \tag{1}$$

$$v(x,z,t) = 0 \tag{2}$$

$$w(x,z,t) = w_0(x,t) \tag{3}$$

where u_0 and w_0 are axial and transverse displacements for the neutral axis, respectively, and ψ_0 is the rotational transverse normal angle about the x-axis. The components of normal (ε_{xx}) and shear (γ_{xz}) strains, using Eqs. (1), (2), and (3), are considered as follows:

$$\varepsilon_{xx} = \frac{\partial u_0}{\partial x} - z\frac{\partial \psi_0}{\partial x}, \tag{4}$$

$$\gamma_{xz} = \frac{\partial w_0}{\partial x} - \psi_0. \tag{5}$$
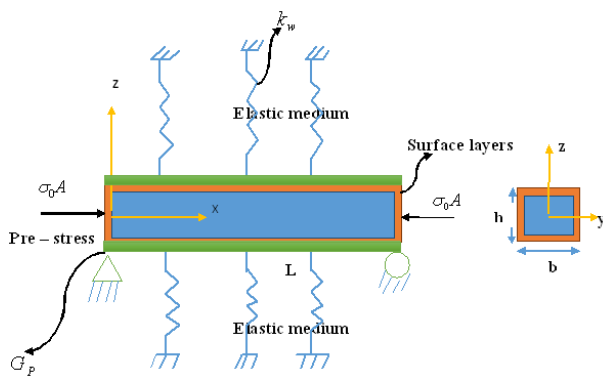
Figure 1. A schematic view of a Timoshenko microbeam model with a surface layer, elastic medium, and pre-stress load.

The strain energy for the linear isotropic elastic material, based on MSGT, is considered as follows [21,22]:

$$U = \frac{1}{2}\int_\Omega (\sigma_{ij}\varepsilon_{ij} + p_i\gamma_i + \tau_{ijk}^{(1)}\eta_{ijk}^{(1)} + m_{ij}\chi_{ij})dV \tag{6}$$

where σ_{ij} and ε_{ij} are the Cauchy stress tensor and the strain tensor, respectively. The expressions γ_i and χ_{ij} denote the dilatation gradient tensor, the deviatoric stretch gradient tensor, and the symmetric rotation gradient tensor, respectively, which are defined as the following forms [23,24]

$$u_{i,j} = \frac{\partial u_i}{\partial x_j} \tag{7}$$

$$\gamma_i = \varepsilon_{mm,i} \tag{8}$$

$$\begin{aligned}\eta_{ijk}^{(1)} = &\frac{1}{3}(\varepsilon_{jk,i} + \varepsilon_{ki,j} + \varepsilon_{ij,k})\\&-\frac{1}{15}\delta_{ij}(\varepsilon_{mm,k} + 2\varepsilon_{mk,m}) - \frac{1}{15}\delta_{ki}(\varepsilon_{mm,j} + 2\varepsilon_{mj,m})\\&-\frac{1}{15}\delta_{jk}(\varepsilon_{mm,i} + 2\varepsilon_{mi,m})\end{aligned} \tag{9}$$

$$\varepsilon_{ij} = \frac{1}{2}(u_{i,j} + u_{j,i}) \tag{10}$$

$$\chi_{ij} = \frac{1}{2}e_{jkl}u_{l,ki} \tag{11}$$

where ε_{mm} and u_i are the dilatation strain and the displacement vector, respectively, according to Akgöz and Civalek [25]. The Knocker symbol is δ_{ij}, and the permutation symbol is e_{ijk}:

$$e_{ijk} = \begin{cases} +1 \text{ for a forwarded permutation of ijk} \\ -1 \text{ for a backwarded permutation of ijk} \\ 0 \text{ if i,j,k is equal} \end{cases} \tag{12}$$

The constitutive equations for linear, elastic, and isotropic materials are given by the following forms [25]

$$\sigma_{ij} = \lambda\delta_{ij}\varepsilon_{mm} + 2\mu\varepsilon'_{ij} \tag{13}$$

$$p_i = 2\mu l_0^2\gamma_i \tag{14}$$

$$\tau_{ijk}^{(1)} = 2\mu l_1^2\eta_{ijk}^{(1)} \tag{15}$$

$$m_{ij} = 2\mu l_2^2\chi_{ij} \tag{16}$$

where ε_{ij}' is the deviatoric strain, which can be written as follows [25]:

$$\varepsilon_{ij}' = \varepsilon_{ij} - \frac{1}{3}\varepsilon_{mm}\delta_{ij} \tag{17}$$

where $l_0, l_1,$ and l_2 denote three additional independent material length scale parameters associated with the dilatation gradient tensor, deviatoric stretch gradient tensor, and symmetric rotation gradient tensor, respectively. In addition, the parameters λ and μ are the Lame coefficients which are given as [26,27]

$$\lambda = \frac{E\upsilon}{(1+\upsilon)(1-2\upsilon)}, \quad \mu = \frac{E}{2(1+\upsilon)} \tag{18}$$

where E and υ denote Young's modulus and Poisson's ratio, respectively.

Using Eqs. (3), (4), and (5), the following equations are given by

$$\gamma_x = \frac{\partial^2}{\partial x^2}u_0 - z\frac{\partial^2}{\partial x^2}\psi_0 \tag{19}$$

$$\gamma_z = -\frac{\partial}{\partial x}\psi_0 \tag{20}$$

Using Eqs. (3), (4), and (5), the nonzero components of the deviatoric stretch gradient tensor $\eta_{ijk}^{(1)}$ can be derived as follows:

$$\begin{aligned}
\eta_{111}^{(1)} &= \frac{2}{5}\frac{\partial^2 u_0}{\partial x^2} - \frac{2}{5}z\frac{\partial^2\psi_0}{\partial x^2}\\
\eta_{333}^{(1)} &= \frac{2}{5}\frac{\partial\psi_0}{\partial x} - \frac{1}{5}\frac{\partial^2 w_0}{\partial x^2}\\
\eta_{113}^{(1)} &= \eta_{131}^{(1)} = \eta_{311}^{(1)} = -\frac{8}{15}\frac{\partial\psi_0}{\partial x} + \frac{4}{15}\frac{\partial^2 w_0}{\partial x^2}\\
\eta_{313}^{(1)} &= \eta_{331}^{(1)} = \eta_{133}^{(1)} = -\frac{1}{5}\frac{\partial^2 u_0}{\partial x^2} + \frac{1}{5}z\frac{\partial^2\psi_0}{\partial x^2}\\
\eta_{122}^{(1)} &= \eta_{212}^{(1)} = \eta_{221}^{(1)} = -\frac{1}{5}\frac{\partial^2 u_0}{\partial x^2} + \frac{1}{5}z\frac{\partial^2\psi_0}{\partial x^2}\\
\eta_{322}^{(1)} &= \eta_{232}^{(1)} = \eta_{223}^{(1)} = \frac{2}{15}\frac{\partial\psi_0}{\partial x} - \frac{1}{15}\frac{\partial^2 w_0}{\partial x^2}
\end{aligned} \tag{21}$$

Substituting Eqs. (19)–(21) into Eq. (11) yields the following form:

$$\chi_{xy} = \chi_{yx} = -\frac{1}{4}(\frac{\partial^2 w_0}{\partial x^2} + \frac{\partial\psi_0}{\partial x}) \tag{22}$$

Using Eqs. (15) and (21), the higher order stresses for MSGT are obtained as the following forms:

$$\begin{aligned}
\tau_{111}^{(1)} &= \frac{4}{5}\mu l_1^2\frac{\partial^2 u_0}{\partial x^2} - \frac{4}{5}\mu l_1^2 z\frac{\partial^2\psi_0}{\partial x^2}\\
\tau_{313}^{(1)} &= \tau_{331}^{(1)} = \tau_{133}^{(1)} = -\frac{2}{5}\mu l_1^2\frac{\partial^2 u_0}{\partial x^2} + \frac{2}{5}\mu l_1^2 z\frac{\partial^2\psi_0}{\partial x^2}\\
\tau_{333}^{(1)} &= \frac{4}{5}\mu l_1^2\frac{\partial\psi_0}{\partial x} - \frac{2}{5}\mu l_1^2\frac{\partial^2 w_0}{\partial x^2}\\
\tau_{113}^{(1)} &= \tau_{131}^{(1)} = \tau_{311}^{(1)} = -\frac{16}{15}\mu l_1^2\frac{\partial\psi_0}{\partial x} + \frac{8}{15}\mu l_1^2\frac{\partial^2 w_0}{\partial x^2}\\
\tau_{122}^{(1)} &= \tau_{212}^{(1)} = \tau_{221}^{(1)} = -\frac{2}{5}\mu l_1^2\frac{\partial^2 u_0}{\partial x^2} + \frac{2}{5}\mu l_1^2 z\frac{\partial^2\psi_0}{\partial x^2}\\
\tau_{322}^{(1)} &= \tau_{232}^{(1)} = \tau_{223}^{(1)} = \frac{4}{15}\mu l_1^2\frac{\partial\psi_0}{\partial x} - \frac{2}{15}\mu l_1^2\frac{\partial^2 w_0}{\partial x^2}
\end{aligned} \tag{23}$$

Using Eqs. (14), (16), (19), (20) and (22), we have

$$\begin{aligned}
m_{xy} &= m_{yx} = -\frac{1}{2}\mu l_2^2(\frac{\partial^2 w_0}{\partial x^2} + \frac{\partial\psi_0}{\partial x})\\
p_x &= 2\mu l_0^2\left(\frac{\partial^2 u_0}{\partial x^2} - z\frac{\partial^2\psi_0}{\partial x^2}\right)\\
p_z &= -2\mu l_0^2\frac{\partial\psi_0}{\partial x}
\end{aligned} \tag{24}$$

The non-zero stresses σ_{ij} are obtained as follows:

$$\begin{aligned}
\sigma_{xx} &= (\lambda + 2\mu)\left(\frac{\partial u_0}{\partial x} - z\frac{\partial\psi_0}{\partial x}\right)\\
\sigma_{xz} &= (k_s\mu)(\frac{\partial w_0}{\partial x} - \psi_0)
\end{aligned} \tag{25}$$

In Eq. (25), k_s denotes the shear correction factor which depends on the shape of microbeam cross-section.

Because of a high surface-to-volume ratio, the surface stress effect plays an important role with micro- and nanoscale materials. For this purpose, the constitutive equation of the Gurtin–Murdoch continuum mechanics approach is considered as follows [28]:

$$\begin{aligned}
\sigma_{\alpha\beta}^s &= \tau_s\delta_{\alpha\beta} + (\tau_s + \lambda_s)\varepsilon_{rr}\delta_{\alpha\beta}\\
&+ 2(\mu_s - \tau_s)\varepsilon_{\alpha\beta} + \tau_s u_{\alpha,\beta}^s\\
\sigma_{\alpha z}^s &= \tau_s u_{z,\alpha}^s
\end{aligned} \tag{26}$$

where τ_s is the residual surface stress under unstrained condition, and μ_s and λ_s are the surface Lame constants. The components of normal and shear surface stress can be written as follows:

$$\begin{aligned}
\sigma_{xx}^s &= \tau_s + (2\mu_s + \lambda_s)\left(\frac{\partial u_0}{\partial x} - z\frac{\partial\psi_0}{\partial x}\right)\\
\sigma_{xz}^s &= \tau_s\frac{\partial w_0}{\partial x}
\end{aligned} \tag{27}$$

The classical beam theory does not satisfy our model. For solving this problem, it is assumed that the stress component σ_{zz} varies linearly through the beam thickness and satisfies the balance conditions on the surfaces. Therefore, σ_{zz} can be written as [28]

$$\sigma_{zz} = \frac{(\frac{\partial \sigma_{xz}^{s+}}{\partial x} - \rho^{s+}\frac{\partial^2 w_0}{\partial t^2}) + (\frac{\partial \sigma_{xz}^{s-}}{\partial x} - \rho^{s-}\frac{\partial^2 w_0}{\partial t^2})}{2} \\ + \frac{(\frac{\partial \sigma_{xz}^{s+}}{\partial x} - \rho^{s+}\frac{\partial^2 w_0}{\partial t^2}) - (\frac{\partial \sigma_{xz}^{s-}}{\partial x} - \rho^{s-}\frac{\partial^2 w_0}{\partial t^2})}{h}z$$

(28)

Using Eq. (27), σ_{zz} can be written as

$$\sigma_{zz} = \frac{2z}{h}\left(\tau_s \frac{\partial^2 w_0}{\partial x^2} - \rho_s \frac{\partial^2 w_0}{\partial t^2}\right)$$

(29)

The normal and shear components, considering bulk and surface effects and using Eq. (29), can be written as

$$\sigma_{xx} = (\lambda + 2\mu)(\frac{\partial u_0}{\partial x} - z\frac{\partial \psi_0}{\partial x}) \\ + \frac{2z\upsilon}{h(1-\upsilon)}(\tau_s \frac{\partial^2 w_0}{\partial x^2} - \rho_s \frac{\partial^2 w_0}{\partial t^2}) \\ \sigma_{xz} = \mu k_s(\frac{\partial w_0}{\partial x} - \psi_0)$$

(30)

Π is the total potential energy that includes the strain energy, kinetic energy, and work done by the external loads, which can written as [4]

$$\Pi = U_{tot} - (K_{tot} + \Omega_{tot})$$

(31)

where

$$U_{tot} = U + U^s \\ K_{tot} = K + K^s \\ \Omega_{tot} = \Omega + V^{elastic}$$

(32)

and where U, U^s, K and K^s are the strain and kinematic energies for bulk and surface effects, respectively. Moreover, Ω and $V^{elastic}$ are the work done by the external forces, including the pre-stress load and the elastic foundation, respectively.

Using Hamilton's principle and a variational method for Timoshenko microbeam model, based on strain gradient theory and the surface stress effects embedded in an elastic medium subjected to pre-stress loading , yields the following equation [4]:

$$\int_0^t [\delta U + \delta U^s - \delta K - \delta K^s - \delta \Omega - \delta V^{elastic}]dt = 0$$

(33)

The surface strain energy is obtained as

$$U^s = \frac{1}{2}\int_0^L \int_s \sigma_{ij}^s \varepsilon_{ij} dSdx$$

(34)

where

$$(A,I) = \int (1,z^2)dA \\ (S,J) = \int (1,z^2)dS$$

Using the presented equations, the strain energy for bulk and surface effects are explained in Appendix A with details. Using Eqs. (14)–(16), the kinetic energy of the Timoshenko microbeam model for bulk and surface effects can be written as

$$k = \int_0^L \int_A \frac{1}{2}\rho(\left(\frac{\partial u}{\partial t}\right)^2 + \left(\frac{\partial w}{\partial t_2}\right)^2)dAdx \\ = \frac{1}{2}\rho[\left(\frac{\partial \psi_0}{\partial t}\right)^2 I + \left(\frac{\partial w_0}{\partial t}\right)^2 A + \left(\frac{\partial u_0}{\partial t}\right)^2 A] \\ k^s = \int_0^L \int_s \frac{1}{2}\rho_s(\left(\frac{\partial u}{\partial t}\right)^2 + \left(\frac{\partial w}{\partial t_2}\right)^2)dSdx \\ = \frac{1}{2}\rho_s[\left(\frac{\partial \psi_0}{\partial t}\right)^2 J + \left(\frac{\partial w_0}{\partial t}\right)^2 S + \left(\frac{\partial u_0}{\partial t}\right)^2 S]$$

(35)

The work done by external forces, including pre-stress load and elastic foundation, can be written as

$$\Omega = \frac{1}{2}\int_0^L (N_{0x}\left(\frac{\partial}{\partial x}w_0\right)^2)dx \\ N_{0x} = \sigma_x^0 A \\ F_{Elastic\ Medium} = k_w w_0 - G_P \nabla^2 w_0 \\ V = \frac{1}{2}\int_0^L (-k_w w_0 + G_P \nabla^2 w_0)w_0 dx$$

(36)

where σ_x^0 is the pre-stress load, and k_w and G_P are Winkler's spring and Pasternak's shear moduli of elastic foundation, respectively.

By substituting Eqs. (A-1), (A-2), (35) and (36) into Eq. (33), one can obtain the governing equations of motion and boundary conditions as follows:

δu_0 :

$$-(bh(\lambda+2\mu)+2(b+h)(\lambda_s+2\mu_s))(\frac{\partial^2}{\partial x^2}u_0)$$
$$+(2I_0^2+\frac{4}{5}I_1^2)\mu bh(\frac{\partial^4}{\partial x^4}u_0)$$
$$+\left(\rho bh+2\rho_s(b+h)\right)(\frac{\partial^2}{\partial t^2}u_0)=0$$

$\delta \psi_0$:

$$(2I_0^2+\frac{4}{5}I_1^2)\frac{\mu bh^3}{12}(\frac{\partial^4}{\partial x^4}\psi_0)$$
$$-(\mu k_s bh+\tau_s(b+h))(\frac{\partial}{\partial x}w_0)$$
$$+\mu k_s bh\psi_0-(\frac{32}{15}I_1^2+\frac{1}{4}I_2^2+2I_0^2)\mu bh(\frac{\partial^2}{\partial x^2}\psi_0)$$
$$+(\frac{16}{15}I_1^2-\frac{1}{4}I_2^2)bh(\frac{\partial^3}{\partial x^3}w_0)$$
$$-((\lambda+2\mu)\frac{bh^3}{12}+(\lambda_s+2\mu_s)(\frac{bh^2}{2}+\frac{h^3}{6}))(\frac{\partial^2}{\partial x^2}\psi_0)$$
$$+(\rho_s(\frac{bh^2}{2}+\frac{h^3}{6})+\rho\frac{bh^3}{12})(\frac{\partial^2}{\partial t^2}\psi_0) \qquad (37)$$
$$-\frac{bh^2\upsilon\tau_s(\frac{\partial^3}{\partial x^3}w_0)}{6(1-\upsilon)}+\frac{bh^2\upsilon\rho_s(\frac{\partial^3}{\partial x^2\partial t}w_0)}{6(1-\upsilon)}=0$$

δw_0 :

$$-(\mu k_s bh+2\tau_s(b+h))(\frac{\partial^2}{\partial x^2}w_0)+(\mu k_s bh$$
$$+\tau_s(b+h))(\frac{\partial}{\partial x}\psi_0)$$
$$-(\frac{16}{15}I_1^2-\frac{1}{4}I_2^2)\mu bh(\frac{\partial^3}{\partial x^3}\psi_0)$$
$$+(\frac{8}{15}I_1^2+\frac{1}{4}I_2^2)\mu bh(\frac{\partial^4}{\partial x^4}w_0)$$
$$+(\rho bh+2\rho_s(b+h))(\frac{\partial^2}{\partial t^2}w_0)$$
$$+N_0(\frac{\partial^2}{\partial x^2}w_0)+k_w w_0-G_P(\frac{\partial^2}{\partial x^2}w_0)$$
$$=0$$

For boundary conditions

δw_0 :

$$(\frac{8}{15}I_1^2+\frac{1}{4}I_2^2)\mu bh(\frac{\partial^3}{\partial x^3}w_0)$$
$$+(\frac{16}{15}I_1^2-\frac{1}{4}I_2^2)\mu bh(\frac{\partial^2}{\partial x^2}\psi_0)$$
$$+(\mu k_s bh+2\tau_s(b+h))(\frac{\partial}{\partial x}w_0)$$
$$-(\mu k_s bh+\tau_s(b+h))\psi_0$$

$\frac{\partial \delta w_0}{\partial x}$:

$$(\frac{8}{15}I_1^2+\frac{1}{4}I_2^2)\mu bh(\frac{\partial^2}{\partial x^2}w_0)-$$
$$(\frac{16}{15}I_1^2-\frac{1}{4}I_2^2)\mu bh(\frac{\partial}{\partial x}\psi_0)$$

δu :

$$(bh(\lambda+2\mu)+2(b+h)(\lambda_s+2\mu_s))(\frac{\partial}{\partial x}u_0)$$
$$-(2I_0^2+\frac{4}{5}I_1^2)\mu bh(\frac{\partial^3}{\partial x^3}u_0)+(b+h)\tau_s$$

$\frac{\partial \delta u}{\partial x}$:

$$(2I_0^2+\frac{4}{5}I_1^2)\mu bh(\frac{\partial^2}{\partial x^2}u_0)$$

ψ :

$$((\lambda+2\mu)\frac{bh^3}{12}+(\lambda_s+2\mu_s)(\frac{bh^2}{2}+\frac{h^3}{6}))(\frac{\partial}{\partial x}\psi_0)$$
$$+(\frac{32}{15}I_1^2+\frac{1}{4}I_2^2+2I_0^2)\mu bh(\frac{\partial}{\partial x}\psi_0)$$
$$-(\frac{16}{15}I_1^2-\frac{1}{4}I_2^2)bh(\frac{\partial^2}{\partial x^2}w_0)$$
$$-(2I_0^2+\frac{4}{5}I_1^2)\frac{\mu bh^3}{12}(\frac{\partial^3}{\partial x^3}\psi_0)$$
$$-\frac{bh^2\tau_s(\frac{\partial^2}{\partial x^2}w_0)}{6(1-\upsilon)}$$

$\frac{\partial \delta \psi}{\partial x}$:

$$(2I_0^2+\frac{4}{5}I_1^2)\frac{\mu bh^3}{12}\left(\frac{\partial^2}{\partial x^2}\psi_0\right)$$

(38)

where

$$A_1 = bh(\lambda + 2\mu) + 2(b+h)(\lambda_s + 2\mu_s)$$

$$A_3 = 2(b+h)\tau_s \qquad A_{13} = bh\mu\kappa_s$$

$$A_7 = (\frac{32}{15}l_1^2 + \frac{1}{4}l_2^2 + 2l_0^2)\mu bh$$

$$A_2 = (\frac{4}{5}l_1^2 + 2l_0^2)\mu bh \quad A_5 = (\frac{16}{15}l_1^2 - \frac{1}{4}l_2^2)\mu bh$$

$$A_6 = (\frac{8}{15}l_1^2 + \frac{1}{4}l_2^2)\mu bh \quad M = (\frac{4}{5}l_1^2 + 2l_0^2)\frac{\mu bh^3}{12} \qquad (39)$$

$$D = (\lambda + 2\mu)\frac{bh^3}{12} + (\lambda_s + 2\mu_s)(\frac{bh^2}{2} + \frac{h^3}{6})$$

$$E = \frac{\upsilon bh^2 \tau_s}{12(1-\upsilon)} \quad G = \frac{\upsilon bh^2 \rho_s}{12(1-\upsilon)}$$

$$I_1 = \rho bh + 2(b+h)\rho_s \quad I_3 = \frac{\rho bh^3}{12} + \rho_s(\frac{bh^2}{2} + \frac{h^3}{6})$$

The dimensionless geometric, mechanical, and surface residual stress, surface mass density, Young's modulus of surface layer, and three material length scale parameters can be defined as follows [28]:

$$U = \frac{u}{L}, W = \frac{w}{h}, X = \frac{x}{L}, \xi = \frac{h}{L},$$

$$\tau = \frac{t}{L}\sqrt{\frac{A_{110}}{I_{10}}}, d = \frac{D}{A_{110}h^2}, I_1^* = \frac{I_1}{I_{10}}, I_3^* = \frac{I_3}{I_{10}h^2}$$

$$g = \frac{G}{I_{10}h^2}, e = \frac{E}{A_{110}h^2}, m = \frac{M}{A_{110}h^4}$$

$$, N = \frac{N_0}{A_{110}}, (a_1, a_3, a_{13}) = \frac{(A_1, A_3, A_{13})}{A_{110}} \qquad (40)$$

$$(a_2, a_5, a_6, a_7) = \frac{(A_2, A_5, A_6, A_7)}{A_{110}h^2},$$

$$K_W^* = \frac{k_w L^2}{A_{110}}, G_P^* = \frac{G_P}{A_{110}}, A_{110} = bh(\lambda + 2\mu), I_{10} = \rho h$$

To use the differential quadrature (DQ) method, first we should convert Eqs. (37) and (38) into dimensionless equations. Thus, substituting Eq. (40) into Eqs. (37) and (38) yields the Eqs. (41a) and (41b).

$\delta U:$

$$-a_1 \frac{\partial^2 U}{\partial X^2} + a_2 \xi^2 \frac{\partial^4 U}{\partial X^4} + I_1^* \frac{\partial^2 U}{\partial \tau^2} = 0$$

$\delta \psi:$

$$a_5 \xi^3 \frac{\partial^3 W}{\partial X^3} - d\xi^2 \frac{\partial^2 \psi}{\partial X^2} + m\xi^4 \frac{\partial^4 \psi}{\partial X^4} + a_{13}\psi$$

$$-a_7 \xi^2 \frac{\partial^2 \psi}{\partial X^2} - a_{13}\xi \frac{\partial W}{\partial X} - g\xi^3 \frac{\partial^3 W}{\partial X \partial \tau^2}$$

$$+e\xi^3 \frac{\partial^3 W}{\partial X^3} - \frac{a_3}{2}\xi \frac{\partial W}{\partial X} + I_3^* \xi^2 \frac{\partial^2 \psi}{\partial \tau^2} = 0 \qquad (41a)$$

$\delta W:$

$$-a_5 \xi^2 \frac{\partial^3 \psi}{\partial X^3} - a_{13}\xi \frac{\partial^2 W}{\partial X^2} + a_6 \xi^3 \frac{\partial^4 W}{\partial X^4}$$

$$+a_{13} \frac{\partial \psi}{\partial X} - a_3 \xi \frac{\partial^2 W}{\partial X^2}$$

$$+\frac{a_3}{2} \frac{\partial \psi}{\partial X} + N\xi \frac{\partial^2 W}{\partial X^2} + K_W^* \xi W$$

$$-G_P^* \xi \frac{\partial^2 W}{\partial X^2} + I_1^* \xi \frac{\partial^2 W}{\partial \tau^2} = 0$$

$$W = 0 \text{ or } a_6 \xi^3 \frac{\partial^3 W}{\partial X^3} + a_5 \xi^2 \frac{\partial^2 \psi}{\partial X^2} + (a_{13} + a_3)\xi \frac{\partial W}{\partial X} - (a_{13} + \frac{a_3}{2})\psi = 0$$

$$\frac{\partial W}{\partial X} = 0 \text{ or } a_6 \xi^2 \frac{\partial^2 W}{\partial X^2} - (a_5 + e)\xi \frac{\partial \psi}{\partial X} = 0$$

$$U = 0 \text{ or } a_1 \frac{\partial U}{\partial X} - a_2 \xi^2 \frac{\partial^3 U}{\partial X^3} + \frac{a_3}{2} = 0$$

$$\frac{\partial U}{\partial X} = 0 \text{ or } \frac{\partial^2 U}{\partial X^2} = 0 \qquad (41b)$$

$$\psi = 0 \text{ or } (d + a_7)\xi \frac{\partial \psi}{\partial X} - (a_5 + e)\xi^2 \frac{\partial^2 W}{\partial X^2} - m\xi^3 \frac{\partial^3 \psi}{\partial X^3} = 0$$

$$\frac{\partial \psi}{\partial X} = 0 \text{ or } \frac{\partial^2 \psi}{\partial X^2} = 0$$

The dimensionless simply supported (SS) boundary conditions for the microbeam model are considered as follows:

$$U = W = (d + a_7)\xi \frac{\partial \psi}{\partial X} - (a_5 + e)\xi^2 \frac{\partial^2 W}{\partial X^2}$$

$$-m\xi^3 \frac{\partial^3 \psi}{\partial X^3} = 0 \qquad (42)$$

3. Using the DQ method to solve the Timoshenko microbeam model

The (DQ) method was used to solve Eq. (41) and the associated boundary conditions in Eq. (42) to determine the free vibration frequencies of the beam. The basic concept of the DQM was defined as the derivative of a function at a given point that can be approximated as a linear sum of a weighted function at all sample points [29,30]. Using this approximation, the differential equations are then reduced to a set of algebraic equations. This approach is convenient for solving problems governed by fourth- or higher-order differential equations.

According to this method, the mth order derivative of the function $f(x)$ with respect to x at a grid point x_i, is approximated by a linear sum of all the functional values in the whole domain as follows [22]:

$$\left.\frac{d^m f}{dx^m}\right|_{x=x_i} = \sum_{j=1}^{N} C_{ij}^{(m)} f(x_j) \tag{43}$$

where x_i is the location of ith sample point in the domain; N is the number of sampling points; $f(x_j)$ is the functional value at point x_i, $C_{ij}^{(m)}$ is the weighting coefficient of the mth order differentiation attached to these functional values. To avoid ill-conditioning, the Lagrange interpolation basis functions are used as the following form [22]:

$$C_{ij}^{(1)} = \begin{cases} \prod_{k=1,k\neq i,j}^{N}(x_i-x_k) / \prod_{k=1,k\neq j}^{N}(x_j-x_k) & (i\neq j) \\ & i,j=1,2,....,N \\ \sum_{k=1,k\neq i}^{N}\frac{1}{(x_i-x_k)} & (i=j) \end{cases} \tag{44}$$

To determine the unequally-spaced positions of the grid points, the Chebyshev–Gauss–Lobatto polynomials were employed as follows [22]:

$$x_i = \frac{L}{2}\left[1-\cos\left(\frac{2i-1}{N-1}\right)\pi\right] \tag{45}$$

The first order weighting matrix can be obtained completely from Eq. (44). Higher-order coefficient matrices can be obtained from the first-order weighting matrix as follows [22]:

$$\begin{aligned} C_{ij}^{(2)} &= \sum_{k=1}^{N} C_{ik}^{(1)} C_{kj}^{(1)} \\ C_{ij}^{(3)} &= \sum_{k=1}^{N} C_{ik}^{(1)} C_{kj}^{(2)} = \sum_{k=1}^{N} C_{ik}^{(2)} C_{kj}^{(1)} \\ C_{ij}^{(4)} &= \sum_{k=1}^{N} C_{ik}^{(1)} C_{kj}^{(3)} = \sum_{k=1}^{N} C_{ik}^{(3)} C_{kj}^{(1)} \end{aligned} \tag{46}$$

Then, substituting Eqs. (44) and (46) into Eqs. (41a) and (42) obtained the following equations of motion using the DQ method

$$\begin{aligned} &-a_1 \sum_{1}^{N} C_{ik}^{(2)} U_k + a_2 \xi^2 \sum_{1}^{N} C_{ik}^{(4)} U_k + I_1^* \frac{\partial^2 U}{\partial \tau^2} = 0 \\ &-(a_5-e)\xi^3 \sum_{1}^{N} C_{ik}^{(3)} W_k - (d+a_7)\xi^2 \sum_{1}^{N} C_{ik}^{(2)} \Psi_k \\ &+m\xi^4 \sum_{1}^{N} C_{ik}^{(4)} \Psi_k + a_{13}\Psi - (a_{13}+\frac{a_3}{2})\xi \sum_{1}^{N} C_{ik}^{(1)} W_k \\ &-g\xi^3 \frac{\partial^2}{\partial \tau^2}(\sum_{1}^{N} C_{ik}^{(1)} W_k) + I_3^* \xi^2 \frac{\partial^2 \Psi}{\partial \tau^2} = 0 \\ &-(a_5)\xi^2 \sum_{1}^{N} C_{ik}^{(3)} \Psi_k - (a_{13}+a_3-N+G_P^*)\xi \sum_{1}^{N} C_{ik}^{(2)} W_k \\ &+a_6\xi^3 \sum_{1}^{N} C_{ik}^{(4)} W_k + (a_{13}+\frac{a_3}{2}) + \sum_{1}^{N} C_{ik}^{(1)} \Psi_k \\ &+K_W \xi W + \frac{\partial^2}{\partial \tau^2}(I_1^* \xi W) = 0 \end{aligned} \tag{47}$$

For (SS) boundary conditions, we have:

$$\begin{aligned} U = W &= (d+a_7)\xi \sum_{1}^{N} C_{ik}^{(1)} \Psi_k - (a_5+e)\xi^2 \sum_{1}^{N} C_{ik}^{(2)} W_k \\ &-m\xi^3 \sum_{1}^{N} C_{ik}^{(3)} \Psi_k = 0 \end{aligned} \tag{48}$$

The general solutions of motion equations are considered as

$$\begin{aligned} U(x,t) &= U(X)e^{i\omega\tau} \\ W(x,t) &= W(X)e^{i\omega\tau} \\ \psi(x,t) &= \psi(X)e^{i\omega\tau} \end{aligned} \tag{49}$$

where $\omega = \sqrt{\frac{I_{10}}{A_{110}}}\Omega L$ is the dimensionless natural frequency. Ω is the fundamental natural frequency, and ρ denotes the density of microbeam.

The stiffness and mass matrices for the Timoshenko microbeam, using strain gradient theory and surface stress effects under pre-stress loading, can be written as

$$\left([\mathrm{K}]-\omega^2[M]\right)\{d_b,d_d\}^T = 0 \tag{50}$$

where $[\mathrm{K}],[M]$ are the stiffness and mass matrices and the subscripts b and d stand for the boundary and domain points, respectively. By solving Eq. (50), the dimensionless natural frequencies for ω and their associated vibration mode shapes can be extracted.

4. Numerical Results and Discussion

The mechanical and geometric properties of a Timoshenko microbeam is considered as [28,31]

$$E = 210 Gpa, \rho = 2331\frac{kg}{m^3}, \upsilon = 0.24,$$

$$\lambda_s = -4.488\frac{N}{m}, \mu_s = -2.774\frac{N}{m}, \tau_s = 0.605\frac{N}{m}$$

$$\rho_s = 3.17e-7\frac{kg}{m^2}, \mathrm{k}_s = 5/6, l = 17.6\mu m$$

$$,b = 2h, h = 4l, \mathrm{L} = 20h, \mathrm{k}_w = 2\times10^4\frac{N}{m}, \mathrm{G}_P = 10\frac{N}{m^2} \tag{51}$$

The material length scale parameter is crucial for the successful application of the MSGT. Dehrouyeh-Semnani and Nikkhah-Bahrami [32] presented an in-depth discussion on how to determine this parameter numerically, and they compared the numerical results obtained to those obtained by experimental testing [32]. They showed the bending rigidity of an epoxy micro-cantilever versus thickness for a modified couple stress model (MCST), using $l = l_c = 17.6\,\mu m$, and the experimental data reported by Lam et al. and found that the results based on the constitutive beam model validated the experimental data, while the Euler-Bernoulli beam model overestimated the bending rigidity of the micro-cantilever. In addition, they depicted that the material length scale parameter of epoxy-based materials on the Euler-Bernoulli beam model equals to $l = l_{EB} = 12.45\,\mu m$. According to the results of Dehrouyeh-Semnani and Nikkhah-Bahrami, the Euler-Bernoulli beam model validated the experimental data very well, but the constitutive beam model underestimated the bending rigidity of the epoxy micro-cantilever. Therefore, in this work, we used the material length scale parameter equal to $17.6\,\mu m$.

Table 1 gives the dimensionless natural frequencies for the Timoshenko microbeam under various boundary conditions. An excellent agreement was found between the present results and the analytical solutions.

The results, obtained by the present work, are compared with the reported results by Ansari et al. [33] in Figure 2, where they demonstrate good agreement each other. In addition, the trend of the results was the same. On the other hand, increasing the aspect ratio (*L/h*) reduced the dimensionless natural frequency. Moreover, the stiffness of the Timoshenko microbeam decreased with increasing the aspect ratio.

Table 1. Comparison of dimensionless natural frequencies with various thicknesses for different boundary conditions.

	Thickness (nm)	S-S	S-C	C-C
Ansari et al. [28]	*h*=1	0.1830	0.2148	0.2524
Present work		0.1863	0.2169	0.2553
Ansari et al. [28]	*h*=5	0.1255	0.1643	0.2117
Present work		0.1258	0.1652	0.2120
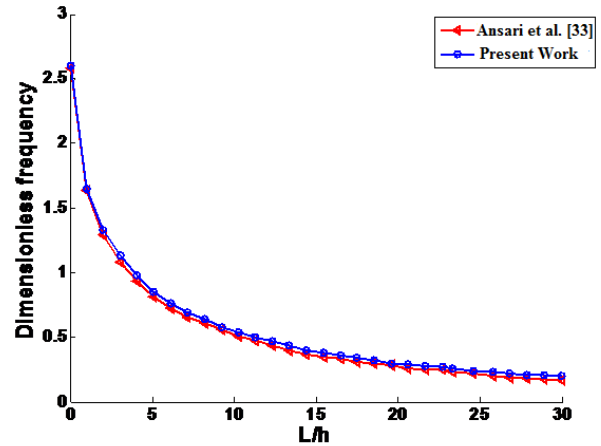
Figure 2. The dimensionless natural frequency versus aspect ratio.

Table 2 shows the first three dimensionless natural frequencies of the Timoshenko microbeam model for the different values of aspect ratio ($\frac{1}{\xi} = \frac{L}{h}$), and surface residual stress (τ_s). As shown in Table 2, by increasing the aspect ratio, the value of the first three dimensionless natural frequencies decreases, and the opposite occurs for the surface residual stress.

The latter subject has been illustrated for dimensionless fundamental natural frequencies in Figure 3. Considering the surface residual stress, the Timoshenko beam at a microscale becomes stiffer, but the effect of this parameter on the dimensionless natural frequency is not noticeable. Therefore, surface residual stress can be ignored in the results.

Table 2. First, second, and third dimensionless natural frequencies of a Timoshenko microbeam model for the different values of $\frac{1}{\xi} = \frac{L}{h}$ and τ_s for ($l_0 = l_1 = l_2 = 1\mu m$).

$\frac{1}{\xi} = \frac{L}{h}$	ω_1	ω_2	ω_3	
10	3.6763	7.3545	11.0340	$\tau_s = 90\left(\frac{N}{m}\right)$
15	3.6387	7.2933	10.9432	
20	3.6208	7.2618	10.8893	
10	3.6762	7.3543	11.0336	$\tau_s = 0\left(\frac{N}{m}\right)$
15	3.6386	7.2931	10.9429	
20	3.6207	7.2616	10.8891	
10	3.6761	7.3540	11.0333	$\tau_s = -90\left(\frac{N}{m}\right)$
15	3.6385	7.2929	10.9426	
20	3.6207	7.2614	10.8888	
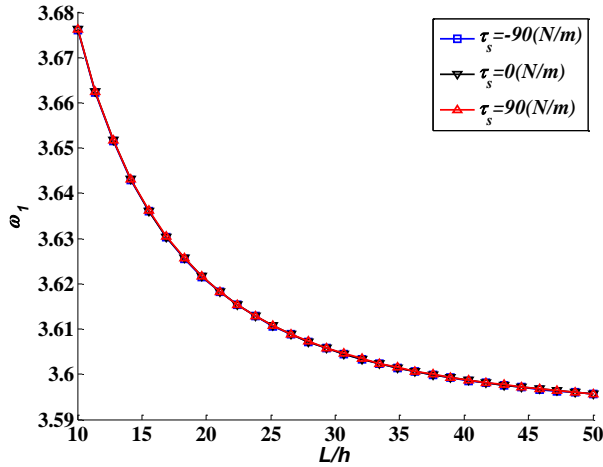
Figure 3. The dimensionless fundamental natural frequency versus aspect ratio for different values of τ_s $(l_0 = l_1 = l_2 = 1\mu m)$
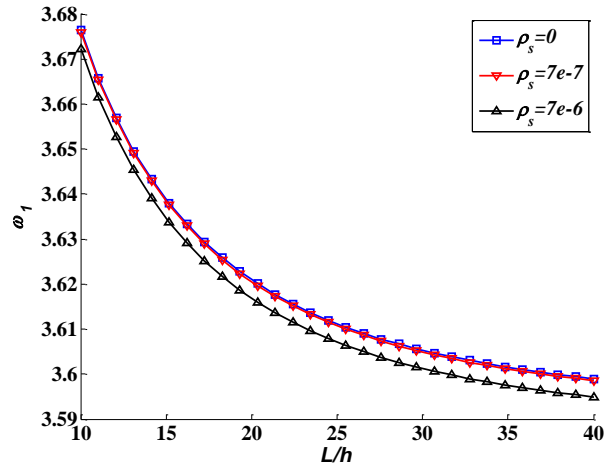
Figure 4. The dimensionless fundamental natural frequency versus aspect ratio for different values of ρ_s $(l_0 = l_1 = l_2 = 1\mu m)$

Tables 3 and 4 depict the first three dimensionless natural frequencies of the Timoshenko microbeam model for the values of the aspect ratio ($\frac{1}{\xi} = \frac{L}{h}$), surface mass density (ρ_s), and Young's modulus of surface layer ($\lambda_s + 2\mu_s$), respectively. By increasing of the $\lambda_s + 2\mu_s$, the value of the first three dimensionless natural frequencies increases and vice versa for surface mass density. A change in $\lambda_s + 2\mu_s$ and ρ_s led to increase stiffness and mass of the micro structure, respectively. Moreover, the results, shown in Figures 4 and 5, are similar to those shown in Tables 3 and 4. Furthermore, Figures 4 and 5 demonstrate that the effect of ρ_s on the dimensionless natural frequency is more than $\lambda_s + 2\mu_s$. However, the effect of $\lambda_s + 2\mu_s$ on the dimensionless natural frequency is not noticeable, and it can be ignored in the results.
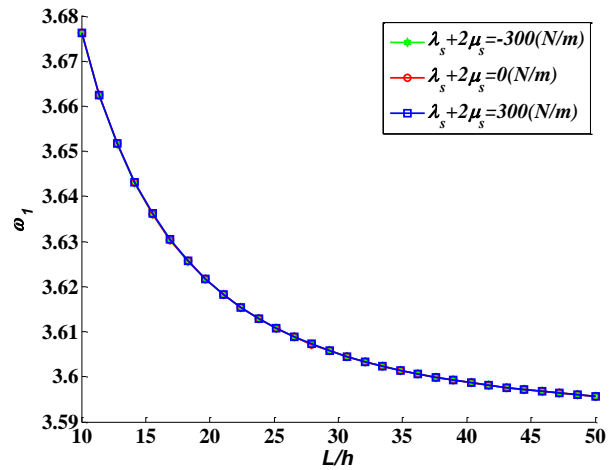
Figure 5. The dimensionless fundamental natural frequency versus aspect ratio for different values of $\lambda_s + 2\mu_s$

$$(l_0 = l_1 = l_2 = 1\mu m)$$

Table 3. First, second, and third dimensionless natural frequencies of the Timoshenko microbeam model for the different values of $\frac{1}{\xi} = \frac{L}{h}$ and ρ_s for $(l_0 = l_1 = l_2 = 1\mu m)$

$\frac{1}{\xi} = \frac{L}{h}$	ω_1	ω_2	ω_3	
10	3.6764	7.3546	11.0342	$\rho_s = 0(\frac{kg}{m^2})$
15	3.6388	7.2935	10.9435	
20	3.6209	7.2620	10.8896	
10	3.6760	7.3538	11.0329	$\rho_s = 7e-7(\frac{kg}{m^2})$
15	3.6383	7.2927	10.9422	
20	3.6205	7.2611	10.8884	
10	3.6722	7.3462	11.0213	$\rho_s = 7e-6(\frac{kg}{m^2})$
15	3.6346	7.2852	10.9309	
20	3.6169	7.2538	10.8772	

Table 4. First, second, and third dimensionless natural frequencies of a Timoshenko microbeam model for the different values of $\frac{1}{\xi} = \frac{L}{h}$ and $\lambda_s + 2\mu_s$ for $(l_0 = l_1 = l_2 = 1\mu m)$

$\frac{1}{\xi} = \frac{L}{h}$	ω_1	ω_2	ω_3	
10	3.6761	7.3541	11.0333	$\lambda_s + 2\mu_s = -300\left(\frac{N}{m^2}\right)$
15	3.6385	7.2930	10.9427	
20	3.6207	7.2615	10.8889	
10	3.6762	7.3543	11.0337	$\lambda_s + 2\mu_s = 0\left(\frac{N}{m^2}\right)$
15	3.6386	7.2931	10.9429	
20	3.6207	7.2616	10.8891	
10	3.6763	7.3544	11.0340	$\lambda_s + 2\mu_s = +300\left(\frac{N}{m^2}\right)$
15	3.6386	7.2932	10.9431	
20	3.6208	7.2617	10.8892	

Figures 6a and 6b show the influence of pre-stress load on the dimensionless first and third natural frequencies versus aspect ratio, respectively. These results demonstrated that the effect of pre-stress load on the greater mode is negligible for higher aspect ratios, and this effect was similar to the lower aspect ratios for all modes. Clearly, the stiffness of microbeam increased at lower aspect ratios. In this figure, the effect of the positive pre-stress load on the natural frequency was higher than that of the negative pre-stress load. Consequently, positive and negative pre-stress loads led to increase and decrease stiffness of the Timoshenko microbeam, respectively. These results are the same for dimensionless natural frequencies.

To consider the size-dependent effects (l denotes the material length scale parameter), the parameter at a microscale is taken into account, and it is non-zero for MSGT ($l_0 = l_1 = l_2 = l$) or MCST ($l_0 = l_1 = 0, l_2 = l$), while at a macro scale, it is zero for CT ($l_0 = l_1 = l_2 = l = 0$).

Figures 7a and 7b are plotted to illustrate the influence of various material length scale theories including modified strain gradient (MSGT) ($l_0 = l_1 = l_2 = l$), modified couple stress (MCST) ($l_0 = l_1 = 0, l_2 = l$), and classical theories (CT) ($l_0 = l_1 = l_2 = 0$) on the dimensionless first and third natural frequencies versus $\frac{h}{l}$, respectively.

Figure 6. The influence of pre-stress load on the dimensionless first (a) and third (b) natural frequencies versus aspect ratios ($N = 0.001$, $N = 0$, $N = -0.001$).
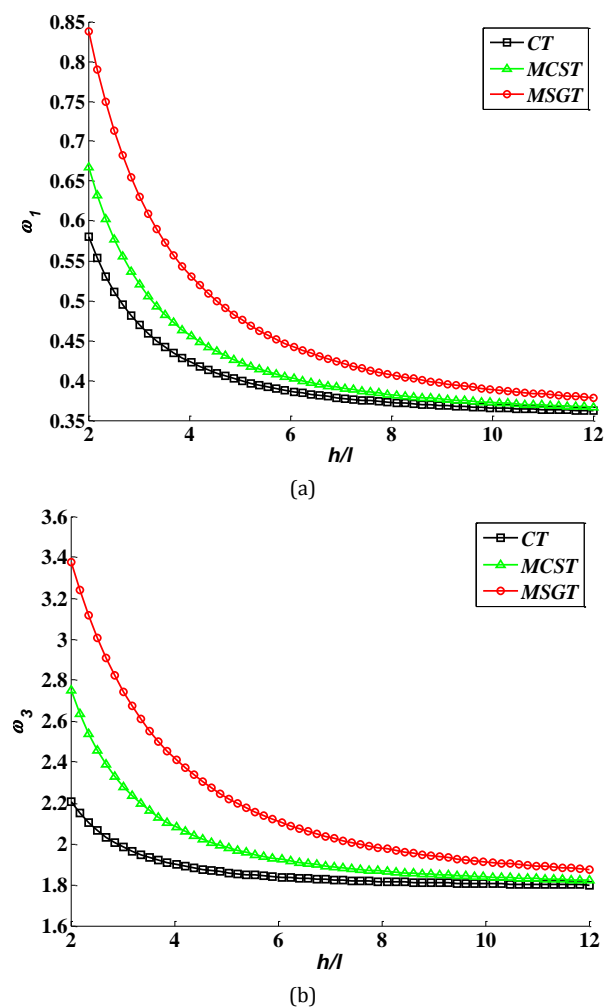
Figure 7. The influence of various material length scale theories on the dimensionless (a) first and (b) third natural frequencies versus h/l.

The effect of the material length scale parameters on the dimensionless natural frequencies for MSGT was higher than that of the other states, such as MCST and CT. This indicates that considering three material length scale parameters $(l_0 = l_1 = l_2 = l)$ led to increase stiffness of the Timoshenko microbeam model, and therefore the dimensionless natural frequencies for MSGT enhanced.

Figures 8 and 9 present the influence of transverse and shear constants of the elastic foundation on the dimensionless fundamental natural frequencies with different values of aspect ratios. The dimensionless natural frequency increased with an increase in the transverse and shear constants of the elastic foundation, while the elastic foundation increased stiffness of the microstructure.
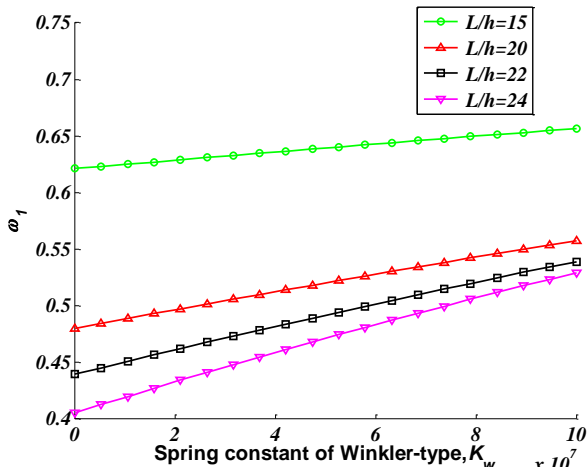
Figure 8. The influence of the transverse constant of the elastic foundation on the dimensionless fundamental natural frequencies with different values of aspect ratios $\frac{1}{\xi} = \frac{L}{h}$, $(G_P = 0)$.
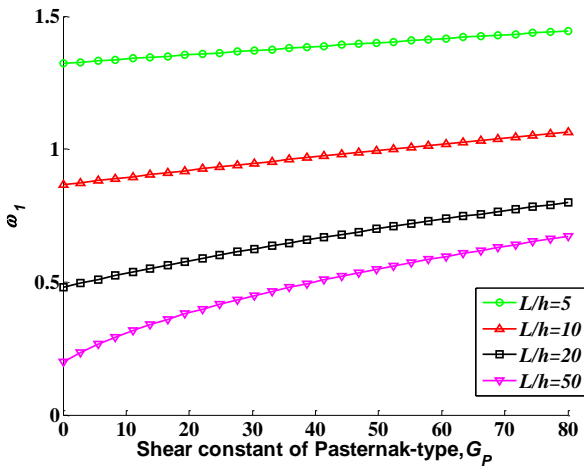
Figure 9. The influence of shear constant of elastic foundation on the dimensionless fundamental natural frequencies with different values of aspect ratios $\frac{1}{\xi} = \frac{L}{h}$, $(k_w = 0)$.

Moreover, increasing the transverse and shear constants of the elastic foundation were directly related to the stiffness of the Timoshenko microbeam and the dimensionless natural frequency.

5. Conclusions

Size-dependent effects on the free vibration analysis of the Timoshenko microbeam model, based on MSGT and surface stress effects subjected to pre-stress loading embedded in an elastic medium, were investigated. The Gurtin–Murdoch continuum mechanical approach was considered, and the set of governing equations were derived using a variational method and solved using DQM. Effects of pre-stress load, surface residual stress, surface mass density, Young's modulus of surface layer, material length scale parameters, and elastic foundation coefficients were studied.

The results of this article can be listed as follows:

- By increasing the aspect ratio, the values of natural frequencies decreased while the opposite occurred for surface residual stress. In addition, when increasing the value of $\lambda_s + 2\mu_s$, the value of the natural frequencies increased, while the surface mass density decreased. Variations in $\lambda_s + 2\mu_s$ and ρ_s led to increase stiffness and mass matrices for the micro structures, respectively. The numerical results showed that the effect of surface residual stress was more than the surface mass density or Young's modulus of the surface layer.

- The effect of pre-stress loading in higher modes was negligible for higher aspect ratios, and this effect was similar to lower aspect ratios across all modes.

- The effect of the three material length scale parameters on the natural frequencies for MSGT was higher than that of the other theories. Application of each of the three material length scale parameters $(l_0, l_1, l_2 \neq 0)$, increased the natural frequencies for MSGT, which was due to the increasing stiffness of the Timoshenko microbeam model.

- Natural frequencies increased with an increase in the transverse and shear constants of the elastic foundation. Consequently, applying the elastic foundation values led to increase stiffness of the Timoshenko microbeam model.

- Comparison between the material length scale parameters and the surface effect confirmed that natural frequencies are more affected by the material length scale parameters than surface effects.

Acknowledgments

References

[1]Ramezani S. A micro scale geometrically non-linear Timoshenko beam model based on strain gradient elasticity theory, *Int J Nonlinear Mech* 2012; 47: 863-73.

[2] Rahaeifard M,Kahrobaiyan MH, Ahmadian MT. Sensitivity analysis of atomic force microscope cantilever made of functionally graded materials; ASME, 2009.

[3] Simsek M, Yurtcu HH. Analytical solutions for bending and buckling of functionally graded-nanobeams based on the nonlocal Timoshenko beam theory, *Compos Struct* 2013; 97: 378-86.

[4] Ghorbanpour Arani A, Kolahchi R, Mosayebi M, Jamali M. Pulsating fluid induced dynamic instability of visco-double-walled carbon nanotubes based on sinusoidal strain gradient theory using DQM and Bolotin method, *Int J Mech Mater Des* 2016; 12: 17-38.

[5] Ghorbanpour Arani A, Dashti P, Amir S,Yousefi M. Nonlinear vibration of coupled nano- and microstructures conveying fluid based on Timoshenko beam model under two-dimensional magnetic field, *Acta Mech* 2015; 226: 2729-60.

[6]Simsek M. Large amplitude free vibration of nanobeams with various boundary conditions based on the nonlocal elasticity theory, *Compos Part B* 2014; 56: 621-28.

[7] Sahmani S, Bahrami M. Size-dependent dynamic stability analysis of microbeams actuated by piezoelectric voltage based on strain gradient elasticity theory, *J Mech Sci Tech* 2015; 29: 325-33.

[8] Mohammadimehr M, Golzari E. The elliptic phenomenon effect of cross section on the torsional buckling of a nanocomposite beam reinforced by a single-walled carbon nanotube, *Proc Instit Mech Eng, Part N: J Nanoeng Nanosys* 2016; 230: 55-67.

[9] Mohammadimehr M, Rahmati AR. Small scale effect on electro-thermo-mechanical vibration analysis of single-walled boron nitride nanorods under electric excitation, *Turkish J Eng, Env Sci* 2013; 37: 1-15.

[10] Atabakhshian V, Shooshtari A, Karimi M. Electro-thermal vibration of a smart coupled nanobeam system with an internal flow based on nonlocal elasticity theory, *Phys B* 2015; 456: 375-82.

[11] Ansari R, Rouhi H, Sahmani S. Free vibration analysis of single- and double-walled carbon nanotubes based on nonlocal elastic shell models, *J Vib Cont* 2014; 20: 670-78.

[12] Akgoz B, Civalek O. A size-dependent shear deformation beam model based on the strain gradient elasticity theory, *Int J Eng Sci* 2013; 70: 1-14.

[13]Asgharifard Sharabiani P, Haeri Yazdi MR. Nonlinear free vibrations of functionally graded nanobeams with surface effects, *Compos Part B* 2013; 45: 581-86.

[14]Ke LL, Wang YS,Wang ZD. Nonlinear vibration of the piezoelectric nanobeams based on the nonlocal theory, *Compos Struct* 2012; 94: 2038-47.

[15] Ansari R, Gholami R, Faghih Shojaei M, Mohammadi V, Sahmani S. Size-dependent bending, buckling and free vibration of functionally graded Timoshenko microbeams based on the most general strain gradient theory, *Compos Struct* 2013; 100: 385-97.

[16] Tounsi A, Al-Basyouni AS, Mahmoud SR. Size dependent bending and vibration analysis of functionally graded microbeams based on modified couple stress theory and neutral surface position, *Compos Struct* 2015; 125: 621-630.

[17] Nazemnezhad R, Salimi M. Hosseini Hashemi SH, Asgharifard Sharabiani P. An analytical study on the nonlinear free vibration of nanoscale beams incorporating surface density effects. *Compos Part B* 2012; 43: 2893-973.

[18] Nejat Pishkenari H, Afsharmanesh B, Akbari E. Surface Elasticity and Size Effect on the Vibrational Behavior of Silicon Nanoresonators, *Current Appl Phys*, 2015; 15: 1389-1396.

[19] Yue YM, Xu KY, Chen T. A micro scale Timoshenko beam model for piezoelectricity with flexoelectricity and surface effects, *Compos Struct* 2016; 136: 278-286.

[20] Preethi K, Rajagopal A, Reddy JN. Surface and Nonlocal Effects for nonlinear analysis of Timoshenko beams, *Int J Nonlinear Mech* 2015; 76: 100-111.

[21] Ke LL, Yang J, Kitipornchai S, Xiang Y. Flexural Vibration and Elastic Buckling of a Cracked Timoshenko Beam Made of Functionally Graded Materials, *Mech Adv Mater Struct* 2009; 16: 488-502.

[22] Mohammadimehr M, Monajemi AA, Moradi M. Vibration analysis of viscoelastic tapered micro-rod based on strain gradient theory resting on visco-pasternak foundation using DQM, *J Mech Sci Tech* 2015; 29: 2297-305.

[23] Kahrobaiyan MH, Asghari M, Ahmadian MT. A strain gradient Timoshenko beam element: application to MEMS, *Acta Mech* 2015, 226: 505-25.

[24] Allahbakhshi A, Allahbakhshi M. Vibration analysis of nano-structure multilayered graphenesheets using modified strain gradient theory, *Front Mech Eng* 2015; 10: 187-97.

[25] Akgoz B, Civalek O. Strain gradient elasticity and modified couple stress models for buckling analysis of axially loaded micro-scaled beams, *Int J Eng Sci* 2011; 49: 1268-80.

[26] Mohammad Abadi M, Daneshmehr AR. An investigation of modified couple stress theory in buckling analysis of micro composite laminated Euler–Bernoulli and Timoshenko beams, *Int J Eng Sci* 2014; 75: 40-53.

[27] Rajabi F, Ramezani S. A nonlinear microbeam model based on strain gradient elasticity theory, *Acta Mech Solida Sinica* 2013; 26: 21-34.

[28] Ansari R, Mohammadi V, Faghih Shojaei M, Gholami R, Sahmani S. On the forced vibration analysis of Timoshenko nanobeams based on the surface stress elasticity theory, *Compos. Part B: Eng* 2014; 60: 158-66.

[29] Ghorbanpour Arani A, Kolahchi R, Khoddami Maraghi Z. Nonlinear vibration and instability of embedded double-walled boron nitride nanotubes based on nonlocal cylindrical shell theory, *Appl Math Model* 2013; 37: 7685-7707.

[30] Murmu T, Pradhan SC. Buckling analysis of a single-walled carbon nanotube embedded in an elastic medium based on nonlocal elasticity and Timoshenko beam theory and using DQM, *Phys E* 2009; 41: 1232-39.

[31] Zhang B, He Y, Liu D, Gan Z, Shen L. Non-classical Timoshenko beam element based on the strain gradient elasticity theory, *Finite Elem Anal Des* 2014; 79: 22-39.

[32] Dehrouyeh-Semnani AM, Nikkhah-Bahrami M. A discussion on evaluation of material length scale parameter based on microcantilever test, *Compos Struct* 2015; 122: 425-429.

[33] Ansari R, Gholami R, Sahmani S. Free vibration analysis of size-dependent functionally graded microbeams based on the strain gradient Timoshenko beam theory, *Compos Struct* 2011; 94: 221-228.

Appendix

The strain energies for bulk and surface effects are written as follows:

$$U = \int_0^L (\frac{1}{2}\lambda A \left(\frac{\partial}{\partial x}u_0\right)^2 + I\mu\left(\frac{\partial}{\partial x}\psi_0\right)^2 + \mu A \left(\frac{\partial}{\partial x}u_0\right)^2$$

$$+ I\mu I_0^2 \left(\frac{\partial^2}{\partial x^2}\psi_0\right)^2 + \frac{1}{2}\mu k_s A \left(\frac{\partial}{\partial x}w_0\right)^2 - \mu k_s A \left(\frac{\partial}{\partial x}w_0\right)\psi_0$$

$$+ \frac{1}{2}\mu k_s \left(\psi_0\right)^2 A + \mu I_0^2 A \left(\frac{\partial^2}{\partial x^2}u_0\right)^2 + \frac{1}{2}I\lambda\left(\frac{\partial}{\partial x}\psi_0\right)^2$$

$$+ \mu I_0^2 A \left(\frac{\partial}{\partial x}\psi_0\right)^2 + \frac{2}{5}I\mu I_1^2 \left(\frac{\partial^2}{\partial x^2}\psi_0\right)^2$$

$$+ \frac{2}{5}\mu I_1^2 A \left(\frac{\partial^2}{\partial x^2}u_0\right)^2 + \frac{16}{15}\mu I_1^2 A \left(\frac{\partial}{\partial x}\psi_0\right)^2 \tag{A-1}$$

$$- \frac{16}{15}\mu I_1^2 A \left(\frac{\partial}{\partial x}\psi_0\right)\left(\frac{\partial^2}{\partial x^2}w_0\right) + \frac{1}{4}\mu I_2^2 A \left(\frac{\partial}{\partial x}\psi_0\right)\left(\frac{\partial^2}{\partial x^2}w_0\right)$$

$$+ \frac{4}{15}\mu I_1^2 A \left(\frac{\partial^2}{\partial x^2}w_0\right)^2 + \frac{1}{8}\mu I_2^2 A \left(\frac{\partial}{\partial x}\psi_0\right)^2 + \frac{1}{8}\mu I_2^2 A \left(\frac{\partial^2}{\partial x^2}w_0\right)^2$$

$$+ \frac{I\upsilon\rho_s\left(\frac{\partial^2}{\partial t^2}w_0\right)\left(\frac{\partial}{\partial x}\psi_0\right)}{(1-\upsilon)h} - \frac{I\upsilon\tau_s\left(\frac{\partial^2}{\partial x^2}w_0\right)\left(\frac{\partial}{\partial x}\psi_0\right)}{(1-\upsilon)h})dx$$

$$U^s = \frac{1}{2}\tau_s\left(\frac{\partial}{\partial x}u_0\right)S + \mu_s\left(\frac{\partial}{\partial x}u_0\right)^2 S + \mu_s J\left(\frac{\partial}{\partial x}\psi_0\right)^2$$

$$+ \frac{1}{2}\lambda_s\left(\frac{\partial}{\partial x}u_0\right)^2 S + \frac{1}{2}\lambda_s J\left(\frac{\partial}{\partial x}\psi_0\right)^2 + \frac{1}{2}\tau_s\left(\frac{\partial}{\partial x}w_0\right)^2 S$$

$$\tag{A-2}$$

$$- \frac{1}{2}\tau_s\left(\frac{\partial}{\partial x}w_0\right)\psi_0 S$$

$$A = bh, \quad I = \frac{1}{12}bh^3, \quad S = 2(b+h), \quad J = \frac{bh^2}{2} + \frac{h^3}{6}$$